

Annual Meeting Selection

Conductivity-depth imaging of helicopter-borne TEM data based on a pseudolayer half-space model

Haoping Huang¹ and Jonathan Rudd²

ABSTRACT

Helicopter-borne time-domain electromagnetic (HTEM) systems with a concentric horizontal coil configuration have been used increasingly in mineral exploration. Conductivity-depth imaging (CDI) is a useful tool for mapping the distribution of geologic conductivity and for identifying conductive targets. A CDI algorithm for HTEM systems with a concentric coil configuration is developed based on the pseudolayer half-space model. Primary advantages of this model are immunity to altimeter errors and better resolution of conductive layers than other half-space models. Effective depth is derived empirically from the diffusion depth and apparent thickness of the pseudolayer. A table lookup procedure is established based on the analytic solution of a half-space model to speed up processing. This efficiency makes generation of real-time conductivity-depth images possible. Tests on synthetic data demonstrate that the pseudolayer conductivity-depth-imaging algorithm maps a wider range of conductivities and does a better job of resolving highly conductive layers, compared with that of the homogeneous half-space model. Effective depths are close to true depths in many circumstances. Field examples show stable and geologically meaningful conductivity-depth images.

INTRODUCTION

Helicopter-borne time-domain electromagnetic (HTEM) systems with a concentric horizontal coil configuration now dominate the airborne electromagnetic industry and are used in mineral exploration, hydrologic projects, and oil and gas programs. In such applications,

conductivity-depth imaging (CDI) of data has proven useful for the distribution of geologic conductivity and for identifying conductive layers within a variably conductive host geology. This approximate technique for interpreting EM data is based on the direct transformation of observed EM data to apparent conductivity and depth. Compared with true inversion methods (e.g., Huang and Palacky, 1991; Chen and Raiche, 1998; Ellis, 1998), CDI algorithms are very efficient because techniques do not require an initial model definition and iterative computations.

There are many techniques for deriving fast conductivity-depth sections from time-domain electromagnetic (TEM) data. The Maxwell receding image concept is commonly used for deriving conductivity from a predicted depth for an image source (e.g., Macnae and Lamontagne, 1987; Nekut, 1987; Macnae et al., 1998). Approximate imaging schemes based on the depth of the maximum current or maximum sensitivity to a layer in a half-space also have been developed (e.g., Eaton and Hohmann, 1989; Fullagar, 1989; Fullagar and Reid, 1992; Smith et al., 1994). Some researchers focused on how to accomplish deconvolutions or decompositions that take into account an arbitrary waveform to estimate the step response of the earth from off-time TEM measurements (e.g., Macnae et al., 1991; Wolfgram and Karlik, 1995; Chen and Macnae, 1998; Eaton, 1998; Stolz and Macnae, 1998). Thin-sheet approaches developed for TEM data also have been used to compute conductance and depth, which can be differentiated into a conductivity-depth section (Macnae et al., 1991; Liu and Asten, 1993; Tartaras et al., 2000). A modification of this method has been introduced to add the possibility of recovering magnetic properties of the geology (Zhdanov and Pavlov, 2001). Still further development of this technique has involved the application of the localized S-inversion (Zhdanov et al., 2002).

Apparent conductivity is typically obtained by transformation of the measured EM response and aircraft altimeter data assuming a half-space model. Techniques were developed by Fraser (1978) for

Presented at the 76th Annual International Meeting, SEG. Manuscript received by the Editor 22 May 2007; revised manuscript received 4 September 2007; published online 1 May 2008.

¹Geo-EM, LLC, Raleigh, North Carolina, U.S.A. E-Mail: haoping_huang@hotmail.com

²Aeroquest, Ltd., Mississauga, Ontario, Canada

© 2008 Society of Exploration Geophysicists. All rights reserved.

frequency-domain systems and by Dyck et al. (1974) and Palacky (1981) for time-domain systems. Figure 1 shows two half-space models in which Figure 1a is termed *homogeneous half-space model* and Figure 1b *pseudolayer half-space model* (Fraser, 1978). The upper (pseudo) layer of the pseudolayer half-space model of Figure 1b is merely an artifact to account for the difference between computed sensor-source distance h and measured sensor altitude a . Measured sensor altitude is determined from the radar or laser altimeter. Any error in the altimeter reading, e.g., an error caused by a forest canopy, falls into the computed sensor-source height and therefore does not corrupt the computed conductivity. In frequency-domain airborne EM methods, the pseudolayer half-space is the model of choice for displaying apparent resistivity in both plan (Fraser, 1990) and sec-

tion (Sengpiel, 1988), partly because of this immunity to altimeter errors. Another merit of the pseudolayer model is better resolution of conductive layers. Furthermore, derived apparent conductivity spans a larger range. These aspects of the model tend to make conductive bedrock layers more recognizable than when the homogeneous half-space model is employed (Fraser, 1978, 1990).

Conductivity transformation of TEM data based on pseudolayer half-space was developed by Palacky (1981), even if he did not specify the point. Based on both Fraser's and Palacky's work, Huang et al. (1983) portrayed explicitly the pseudolayer technique for airborne TEM systems. However, techniques reported in the early 1980s yielded a single conductivity from all channel data and were used for conductivity mapping rather than for depth sounding.

We present an approach to CDI using a pseudolayer half-space model. The concept of the effective depth is used. The new algorithm, as applied to HTEM data, is tested on synthetic and field data with encouraging results.

AEROTEM SYSTEMS

The original concept of a coincident coil HTEM system was pioneered by Aerodat scientists in the early 1980s under Wally Bokyo's guidance. Since then, Aeroquest has refined the system design into an effective and fieldworthy exploration tool that is optimized to provide the maximum amount of information on a target conductor. The transmitter consists of a large loop towed by a helicopter with receivers located at the center of the transmitter loop. Diameter of the transmitter loop can be 5 m, 9 m, or 12 m. The transmitter waveform is a bipolar symmetric triangular pulse which can be operated at 150, 90, and 30 Hz with a 30–50% duty cycle. The transmitter moment is $4 \times 10^4 \text{ Am}^2$ for the 5-m system and $2.3 \times 10^5 \text{ Am}^2$ for the 12-m system. Vertical and inline horizontal components of induced voltage of the secondary magnetic fields are measured during transmitter on time and off time. There are 16 on-time channels plus 17 off-time channels for both components. Finite transmitter turnoff time might affect TEM data collected at times shortly after transmitter turnoff when transmitter turnoff time is large (Fitterman and Anderson, 1984). AeroTEM systems allow sufficient time between transmitter turnoff and first time-off data sampling to avoid the effects of transmitter turnoff. Strengths of AeroTEM systems include high spatial resolution, broadband response, source geometry discrimination, and depth of investigation.

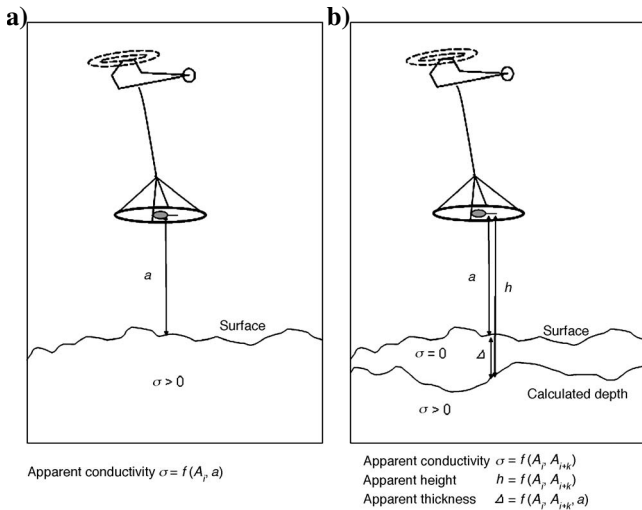


Figure 1. Sketch of the HTEM system and half-space models. Transmitter consists of a large loop towed by a helicopter with receivers located at the center of the transmitter loop. (a) Homogeneous half-space model in which the top of the half-space coincides with earth's surface, as defined by radar or laser altimeter. (b) Pseudolayer half-space model in which the top of the half-space is defined numerically by output parameter h . The pseudolayer half-space model is equivalent to a two-layer case in which the upper layer is of zero conductivity. Thickness Δ is the difference between interpreted height h and bird altitude a as obtained from the altimeter.

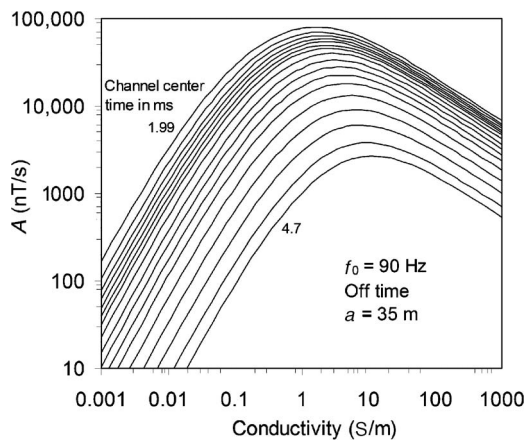


Figure 2. Seventeen channel off-time responses to a homogeneous half-space for 12-m bird at a height of 35 m. Base frequency $f_0 = 90 \text{ Hz}$.

METHOD

A sketch of the HTEM system and half-space models is shown in Figure 1. The transmitter consists of the large loop towed by a helicopter and the horizontal and vertical component receiver coils located at the center of the transmitter loop. For concentric transmitting and receiving coils, the half-space response in the frequency domain can be found in Ward and Hohmann (1988). This response can be Fourier-transformed to the time-domain. Figure 2 depicts the off-time response A to a half-space as a function of conductivity σ . The response for each channel, given in nT/s, increases with increasing conductivity at low conductivities, reaches a peak at moderate conductivity (about 1 S/m), and then decreases as σ continues to increase.

Figure 2 shows that conductivity cannot be determined uniquely from a single channel of data but can be derived from any two chan-

nels. Assuming decay curves can be approximated as a piecewise exponential function of time, we can calculate the time constant, τ_i , from two channels as

$$\tau_i = \frac{t_{i+k} - t_i}{\ln\left(\frac{A_i}{A_{i+k}}\right)}, \quad (1)$$

where t_i and A_i are the center time and measured response in nT/s for the i th channel, respectively, and k (≥ 1) is the channel interval used to calculate τ_i , which can be 1 for high-quality data and as much as 4 for low-quality data.

Then we define the amplitude α_i to be

$$\alpha_i = (A_i^2 + A_{i+k}^2)^{1/2}. \quad (2)$$

Apparent conductivity σ_a and apparent bird height h can be computed from a pair of τ_i and α_i . Apparent thickness Δ of the pseudolayer (= depth to top of half-space) can be calculated from h and measured bird altitude a , i.e., $\Delta = h - a$. If N channels of data are available, $N-k$ apparent conductivities and apparent thicknesses can be computed.

In practice, we create a lookup table to compute σ and h based on analytic solutions to speed up the process. This procedure is understood easily by using a graphical presentation shown in Figure 3. A diagram is used to yield a unique σ and h from each pair of τ_i and α_i . For measured data, we calculate τ_i and α_i from channel i and channel $i + k$. These pairs, τ_i and α_i , then locate a point on a corresponding diagram such as Figure 3, which is one of the $N-k$ diagrams. The point determines conductivity σ and height h . Solutions are interpolated in which the location does not fall directly on conductivity-altitude curves. If the earth is truly homogeneous, the conductivity obtained from Figure 3 is equal to the true conductivity σ . When it is not homogeneous, the solution is an apparent conductivity σ_a .

Conductivity σ_i of channel i will be associated with an effective depth d_i that we determine next. We begin with the time-domain diffusion depth, which is proportional to the square root of sampling time t_i and inverse conductivity σ_i . Thus, we write

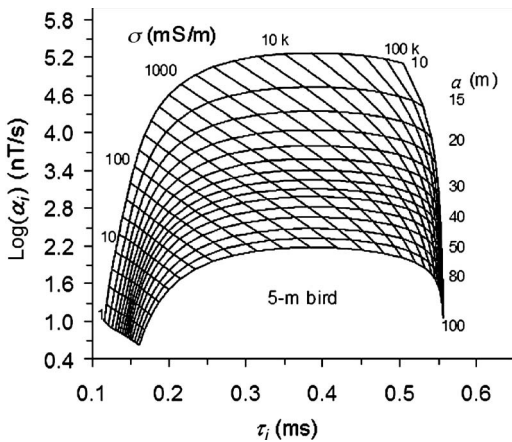


Figure 3. Diagram of time constant τ_i and amplitude α_i (in logarithmic space) of half-space model for two time-off channels.

$$\delta_i = \left(\frac{2t_i}{\sigma_i\mu_0}\right)^{1/2}, \quad (3)$$

where μ_0 is the magnetic permeability of free space. Because the pseudolayer model is used, effective depth is related to apparent thickness and can be written generally as

$$d_i = f(\delta_i, \Delta_i) \quad (4)$$

(Huang and Fraser, 1996), where the function itself is determined empirically based on experimentation with synthetic data. Figure 4 provides a graphic presentation of our choice of the effective depth as a function of δ_i and Δ_i .

Tests on synthetic data

We have compared output of the homogeneous half-space and pseudolayer half-space algorithms for a variety of layered earth examples. We refer to apparent conductivities obtained from the homogeneous half-space model as homogeneous conductivity and those from the pseudolayer model as pseudolayer conductivity. Algorithms were tested on synthetic data obtained from a series of homogeneous half-space models in which testing yielded output conductivities from the homogeneous algorithm and conductivities and pseudolayer thicknesses from the pseudolayer algorithm. Conductivity returned for each channel pair yielded errors generally less than 0.1%, and computed pseudolayer thicknesses were all 0 ± 0.1 m. Having established the efficacy of algorithms for a half-space, we now apply them to a variety of multilayer earth synthetic data to determine their usefulness in yielding CDIs that are reflective of layering in the earth.

In the following examples, synthetic data were computed using AeroTEM 5-m system data and parameters. Width of the transmitted pulse is 1.1 ms, and 17 off-time data channels were used for soundings with $k = 3$ for pseudolayer conductivity. Because model studies were conducted using layered-earth models, only the vertical component is considered.

We first examine two two-layer cases, one of which has a resistive upper layer (Figure 5a) and the other a conductive upper layer (Figure 5b). In both cases, the upper layer is 100 m thick. The first model (Figure 5a) has a surface-layer conductivity of 10 mS/m and basement conductivity of 100 mS/m. The second model (Figure 5b) has a surface-layer conductivity of 100 mS/m and basement conductivity of 10 mS/m. Apparent conductivities are computed using the ho-

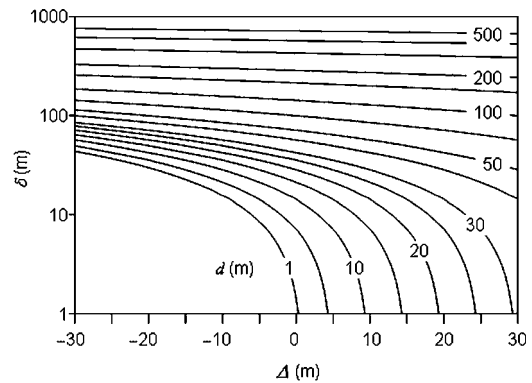


Figure 4. The effective depth computed from an empirical as a function of δ and Δ .

mogeneous and pseudolayer models. Analogous to findings in the frequency-domain case, conductive targets at depth are imaged better by using the pseudolayer method, whereas the homogeneous half-space method tends to represent near-surface conductivity better (Fraser, 1978, 1990). Figure 5a shows that pseudolayer conductivity is closer to the true value of the conductive basement than homogeneous conductivity is. In Figure 5b, the presence of the resistive basement is indicated somewhat by pseudolayer conductivity, whereas it is indicated very poorly by homogeneous conductivity.

We now examine the response to three-layer cases. Figure 6a displays a conductive thin layer (200 mS/m, 20 m thick) underlying a moderately resistive cover (20 mS/m, 100 m thick) with a resistive basement (2 mS/m). Figure 6b illustrates a 20-m-thick resistive layer (5 mS/m) sandwiched in a conductive host (50 mS/m) at 100-m depth. Pseudolayer conductivity, shown in Figure 6a, clearly indicates a three-layer earth, whereas the homogeneous conductivity algorithm fails to indicate the resistive basement. Pseudolayer conductivity is not significantly superior to homogeneous conductivity in the case of a resistive middle layer (Figure 6b), illustrating the difficulty of detecting thin resistive layers with EM.

Figure 7 depicts results from a four-layer earth with conductivities 100-2-500-2 mS/m reflecting conductive overburden on a resistive

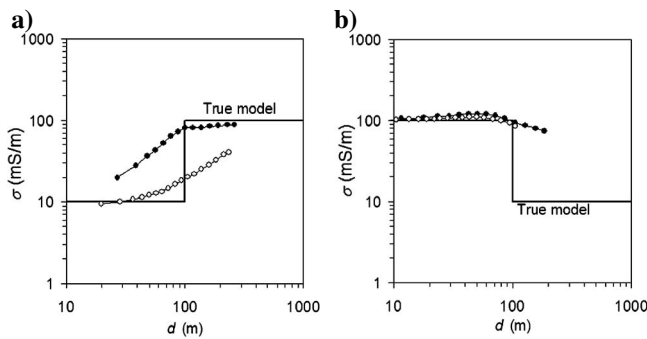


Figure 5. Conductivity-depth diagrams for two-layer models. First layer thickness is 100 m. Layer conductivities are (a) 10 and 100 mS/m and (b) 100 and 10 mS/m. The straight lines are true model conductivities, the curves with solid circles are pseudolayer conductivities, and the curves with open circles are homogeneous conductivities.

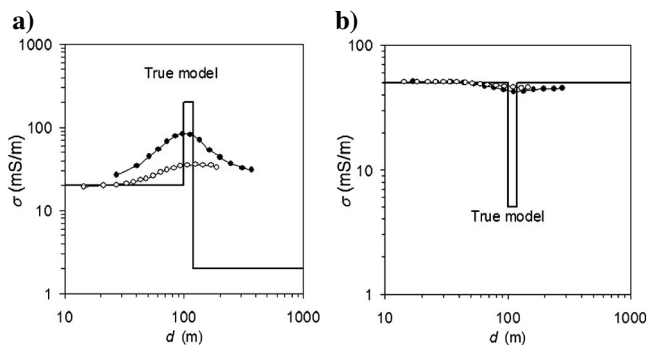


Figure 6. Conductivity-depth diagrams for two three-layer models. Layer conductivities from the surface to depth are (a) 20, 200, and 2 mS/m and (b) 50, 5, and 50 mS/m. The first layer is 100 m thick, and the second layer is 20 m thick. The straight lines are true model conductivities, the curves with solid circles are pseudolayer conductivities, and the curves with open circles are homogeneous conductivities.

host containing a conductive target layer. The thin conductive layer (10 m) is at 100-m and 200-m depths in Figure 7a and b, respectively. Curves for both the homogeneous and pseudolayer algorithms indicate qualitatively that a four-layer earth exists when the thin conducting layer is shallower (Figure 7a). When the depth to the thin layer is increased to 200 m, we cannot detect the resistive basement from homogeneous conductivity. However, the pseudolayer curve rapidly follows sharp changes in conductivity at layer interfaces, thereby indicating existence of resistive material below the conductor.

We now simulate an isolated conducting lens-shaped object in a moderately resistive host. Conductivity of the lens-shaped object is 200 mS/m, and thickness at its center is 25 m. The lens is located at the center of the profile at a 180-m depth in a 20 mS/m host. Synthetic data are computed from a series of 1D models to form a data profile shown in Figure 8a. Responses over the object are lower than those of the background for early-time channels because of over-

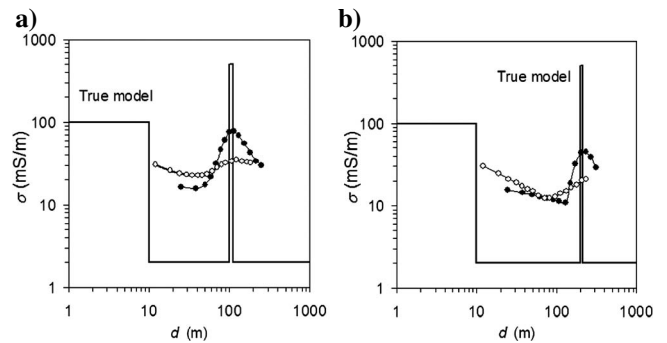


Figure 7. Conductivity-depth diagrams for two four-layer models. Layer conductivities from the surface to depth are 100, 2, 500, and 2 mS/m. The first layer is 10 m thick. The thin conductive third layer is 10 m thick. Depth to this layer is (a) 100 m and (b) 200 m, respectively. The straight lines are true model conductivities, the curves with solid circles are pseudolayer conductivities, and the curves with open circles are homogeneous conductivities.

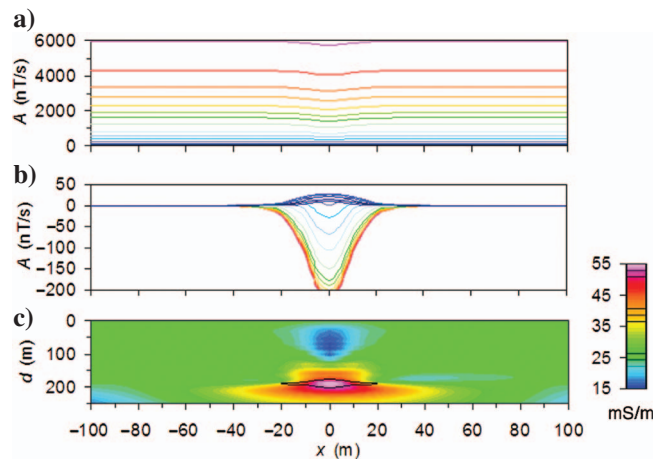


Figure 8. A conductive lenslike object (200 mS/m) in a moderately resistive host (20 mS/m). Top of lens is 180 m deep. Maximum thickness of lens is 25 m. (a) Synthetic responses computed from a series of 1D models. (b) Synthetic response with background response removed. Warm colors indicate early-time channels and cool colors late-time channels. (c) Imaged conductivity-depth section with lens outlined.

shoot/undershoot effects which commonly are seen in electrical soundings. A positive anomaly is shown on later-time channels. These can be seen clearly by removing the background response, as presented in Figure 8b. We added 5% random noise to the synthetic data and then computed pseudolayer conductivities and depths. The resulting conductivity-depth image is illustrated in Figure 8c, with the lens-shaped object outlined in black.

Finally, we consider a resistive lens-shaped object (5 mS/m) in a moderately conductive host (20 mS/m). The depth to the top of the lens is 50 m, and thickness at the center of the lens is 80 m. Figure 9 shows synthetic responses with and without background and the conductivity-depth section. Responses above the lens are lower than that of the background for all time channels because of the resistive object at depth.

Field examples

Data for the following two field examples were collected using an AeroTEM system. The first example is from an area where a variable layer of conductive overburden occurs over a resistive geology. Figure 10 shows off-time data from a 23-km line and resulting CDI section. Much of the line has a high-amplitude, rapidly decaying response typical of a thin conductive surface layer. This response appears to be modeled correctly in CDI as a near-surface conductive

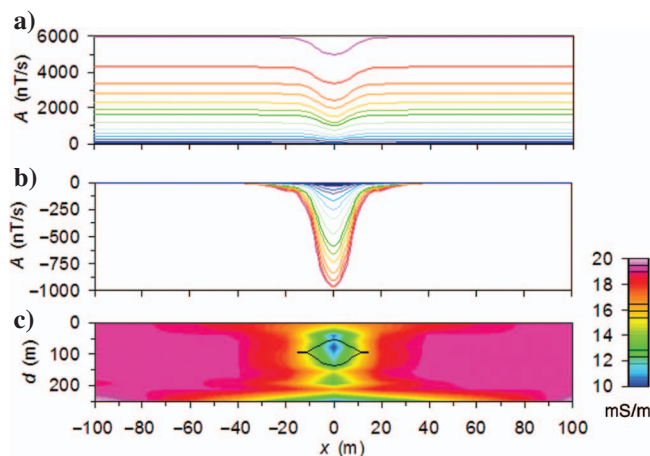


Figure 9. A resistive lenslike object (5 mS/m) in a moderately conductive host (20 mS/m). Top of lens is 50 m deep. Lens thickness is 80 m. (a) Synthetic responses computed from a series of 1D models. (b) Synthetic response with background response removed. Warm colors indicate early-time channels and cool colors late-time channels. (c) Imaged conductivity-depth section with lens outlined.

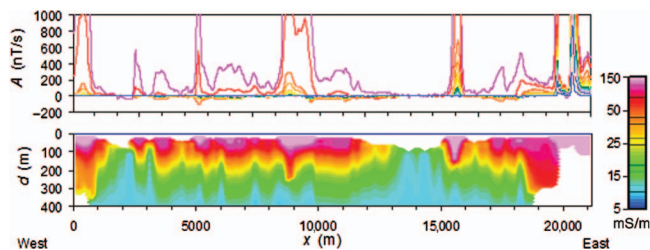


Figure 10. HTEM data obtained from a resistive area and CDI section. Warm colors indicate early-time channels, and cool colors indicate late-time channels.

layer. This data set, which comprises more than 10,000 data points, took only a few seconds to process for apparent conductivities and depths.

The second AeroTEM field example is from the oil sands area in northern Alberta, Canada. The survey was flown with 250-m line spacing in an east-west orientation. CDI sections were computed for all lines, and a conductivity volume was constructed by interpolating results from section to section across the survey area. Figure 11 depicts the CDI volume. The more conductive zones are shown in cooler colors, and resistive geology is shown in warmer colors.

Conductive shales of the Clearwater Formation overlie McMurray Formation sandstone (reservoir rock). Both units have a shallow easterly dip across the survey area. The top edge of the Clearwater Formation can be seen in the far northwestern corner of the block where the resistive McMurray Formation is at surface. Conductivity

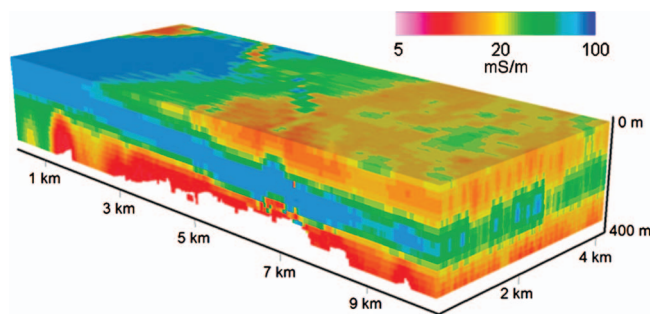


Figure 11. CDI volume computed from AeroTEM data obtained from an oil-sands area in Alberta, Canada.

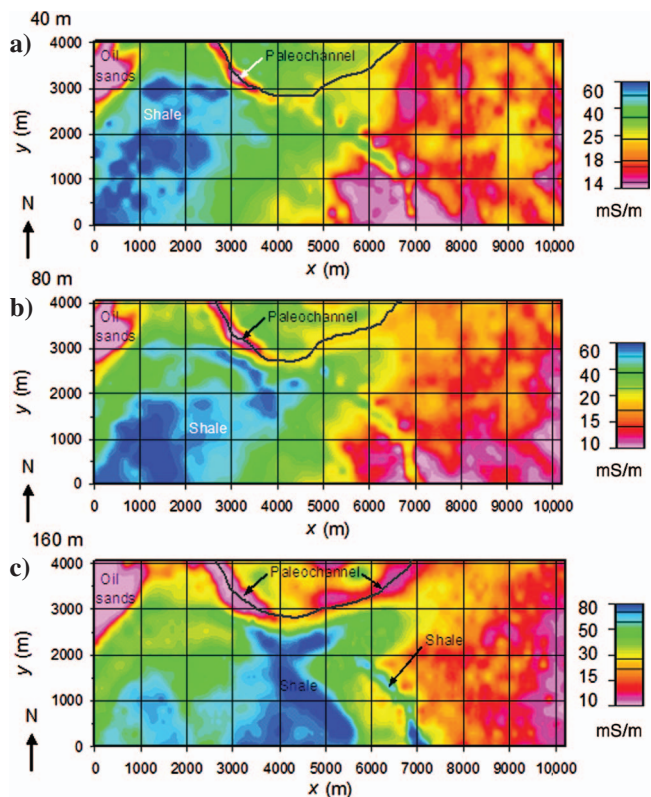


Figure 12. Three apparent conductivity-depth slices at (a) 40 m, (b) 80 m, and (c) 160 m based on CDI results.

imaging has identified a variably conductive near-surface layer in the eastern half of the survey area. Resistive portions of this layer correlate well with known aggregate accumulations. A paleochannel can be seen clearly, based on morphology in the northern portion of the survey block. CDI indicates that the channel is filled with relatively resistive sediment.

Three depth-slice plan images at depths of 40 m, 80 m, and 160 m are shown in Figure 12. Conductivity maps, which can be produced for any depth from CDI results, are an effective way of visualizing conductive layers and features in plan view at various depths. The conductive shale unit shown in cooler colors dips gently to the east. Resistive channels clearly stand out in northwestern and northern areas ($x = 2500\text{--}7000$ m and $y = 2900\text{--}4000$ m), probably cutting entirely through the shale unit in the northwest. More resistive areas which overlie shales are likely to reflect potential aggregate sources. The resistive area in and around $x = 6200$ m and $y = 500$ m is a known accumulation of approximately 120 m of sandy overburden. When combined with even sparse drilling information, HTEM data are very useful in mapping various geologic features in this environment.

CONCLUSIONS

An algorithm has been developed for transforming HTEM data to apparent conductivity and effective depth based on the pseudolayer half-space model. Compared with the homogeneous half-space model, there are two advantages of the pseudolayer technique — immunity to altimeter errors and better identification and resolution of conductive layers. A table lookup procedure is issued based on the analytic solution to the pseudolayer half-space model to speed up processing. This makes real-time processing of conductivity-depth images possible. Tests on synthetic data demonstrate that pseudolayer conductivity is sensitive to a wider range of conductivities and does a better job of resolving good conductors. The effective depth derived empirically from diffusion depth and apparent thickness of the pseudolayer is close to true depth in a wide range of circumstances. Field examples show stable and geologically meaningful conductivity-depth sections.

ACKNOWLEDGMENTS

The authors thank Associated Mining Consultants Ltd., Calgary, Alberta, Canada, for valuable contributions to this paper. Appreciation is expressed to David Fitterman and Douglas Fraser for constructive reviews that greatly helped improve this paper. In addition, appreciation is expressed to editors and anonymous reviewers for their valuable comments and suggestions.

REFERENCES

Chen, J., and J. C. Macnae, 1998, Automatic estimation of EM parameters in tau-domain: *Exploration Geophysics*, **29**, 170–174.

- Chen, J., and A. Raiche, 1998, Inverting AEM data using a damped eigenparameter method: *Exploration Geophysics*, **29**, 128–132.
- Dyck, A. V., A. Becker, and L. S. Collett, 1974, Surficial conductivity mapping with the airborne INPUT system: *Canadian Institute of Mining and Metallurgical Bulletin*, **67**, 104–109.
- Eaton, P. A., 1998, Application of an improved technique for interpreting transient electromagnetic data: *Exploration Geophysics*, **29**, 175–183.
- Eaton, P. A., and G. W. Hohmann, 1989, A rapid inversion technique for transient electromagnetic soundings: *Physics of the Earth and Planetary Interiors*, **53**, 384–404.
- Ellis, R. G., 1998, Inversion of airborne electromagnetic data: *Exploration Geophysics*, **29**, 121–127.
- Fitterman, D. V., and W. L. Anderson, 1984, Effect of transmitter turnoff characteristics on transient soundings: 54th Annual International Meeting, SEG, Expanded Abstracts, 69–71.
- Fraser, D. C., 1978, Resistivity mapping with an airborne multicoil electromagnetic system: *Geophysics*, **43**, 144–172.
- , 1990, Layered-earth resistivity mapping, in D. V. Fitterman, ed., *Developments and applications of modern airborne electromagnetic surveys: United States Geological Survey Bulletin*, 1925, 33–41.
- Fullagar, P. K., 1989, Generation of conductivity-depth pseudo-sections for coincident loop and in-loop TEM data: *Exploration Geophysics*, **20**, 43–45.
- Fullagar, P. K., and J. E. Reid, 1992, Conductivity-depth transformations of fixed loop TEM data: *Exploration Geophysics*, **23**, 515–520.
- Huang, H., and D. C. Fraser, 1996, The differential parameter method for multifrequency airborne resistivity mapping: *Geophysics*, **61**, 100–109.
- Huang, H., and G. J. Palacky, 1991, Damped least-squares inversion of time domain airborne electromagnetic data based on singular value decomposition: *Geophysical Prospecting*, **39**, 827–844.
- Huang, H., H. Xi, Y. Wang, D. Zhu, and H. Piao, 1983, Transformation of the time-domain airborne electromagnetic response to apparent resistivity and its application in geological mapping: *Journal of Changchun College of Geology*, **3**, 135–144.
- Liu, G., and M. Asten, 1993, Conductance-depth imaging of airborne TEM data: *Exploration Geophysics*, **24**, 655–662.
- Macnae, J. C., A. King, N. Stolz, A. Osmakoff, and A. Blaha, 1998, Fast AEM data processing and inversion: *Exploration Geophysics*, **29**, 163–169.
- Macnae, J., and Y. Lamontagne, 1987, Imaging quasi-layered conductive structures by simple processing of transient electromagnetic data: *Geophysics*, **52**, 545–554.
- Macnae, J. C., R. Smith, B. D. Polzer, Y. Lamontagne, and P. S. Klinkert, 1991, Conductivity-depth imaging of airborne electromagnetic step-response data: *Geophysics*, **56**, 102–114.
- Nekut, A. G., 1987, Direct inversion of time-domain electromagnetic data: *Geophysics*, **52**, 1431–1435.
- Palacky, G. J., 1981, The airborne electromagnetic method as a tool of geological mapping: *Geophysical Prospecting*, **29**, 60–88.
- Sengpiel, K. P., 1988, Approximate inversion of airborne EM data from a multilayered ground: *Geophysical Prospecting*, **36**, 446–459.
- Smith, R. S., R. N. Edwards, and G. Buselli, 1994, Automatic technique for presentation of coincident-loop, impulse-response, transient, electromagnetic data: *Geophysics*, **59**, 1542–1550.
- Stolz, E. M., and J. C. Macnae, 1998, Evaluating EM waveforms by singular-value decomposition of exponential basis functions: *Geophysics*, **63**, 64–74.
- Tartaras, E., M. S. Zhdanov, K. Wada, A. Saito, and T. Hara, 2000, Fast imaging of TDEM data based on S-inversion: *Journal of Applied Geophysics*, **43**, 15–32.
- Ward, S. H., and G. W. Hohmann, 1988, Electromagnetic theory for geophysical applications, in M. N. Nabighian, ed., *Electromagnetic methods in applied geophysics*, v. 1, Theory: SEG, 130–311.
- Wolfgang, P., and G. Karlik, 1995, Conductivity-depth transform of GEOTEM data: *Exploration Geophysics*, **26**, 179–185.
- Zhdanov, M. S., and D. A. Pavlov, 2001, Analysis and interpretation of anomalous conductivity and magnetic permeability effects in time domain electromagnetic data: Part II: $S\mu$ -inversion: *Journal of Applied Geophysics*, **46**, 235–248.
- Zhdanov, M. S., D. A. Pavlov, and R. Ellis, 2002, Localized S-inversion of time domain electromagnetic data: *Geophysics*, **67**, 1115–1125.